

Characterization of Chain Molecular Assemblies in Long-Chain, Layered Silver Thiolates: A Joint Infrared Spectroscopy and X-ray Diffraction Study

A. N. Parikh,^{*,†} S. D. Gillmor,^{†,||} J. D. Beers,^{†,||} K. M. Beardmore,[‡] R. W. Cutts,^{§,||} and B. I. Swanson^{*,†}

Chemical Science & Technology, Materials Science & Technology, and Theoretical Divisions, Los Alamos National Laboratory, Los Alamos, New Mexico 87545

Received: October 1, 1998; In Final Form: February 1, 1999

The first direct characterization of structures of bi-molecular chain assemblies in a self-consistent series of pillared, layered organic–inorganic long-chain silver (*n*-alkane) thiolates, (AgS(CH₂)_{*n*}CH₃; *n* = 5, 6, 9, 11, 15, and 17), is reported using the combined application of infrared transmission spectroscopy and powder X-ray diffraction. The structural attributes elucidated include quantitative estimates of average chain orientation, chain conformation, chain–chain translational order, interpenetration of the contiguous layers, as well as void characteristics in the chain matrix. The evidence presented here establishes that the layered chain assemblies sandwiched between the inorganic Ag–S backbones in a double-layer arrangement are comprised of an ordered packing of all-trans-extended chains. The average chain in each assembly is oriented vertically away from the quasi-hexagonal Ag–S lattice, in a two-dimensional pseudo-monoclinic arrangement of domains of 60–70 translationally correlated chains. Small interpenetration between the contiguous layers leads to the formation of regularly spaced 1D channels or corridors. The three-dimensional network of 1D channels alternates between the chain layers. All the chain structural characteristics deduced here are in good conformity with those implied in the model proposed earlier by Dance and co-workers. The present results, together with the previous X-ray analysis for comparable short-chain AgSRs, are used to propose a two-step, hierarchical self-assembly mechanism for the formation of silver (*n*-alkyl) thiolates. It is proposed that the primary self-assembly process involves the organization of Ag⁺ and RS[−] species into puckered sheets of quasi-hexagonally symmetric 2D lattices, with the chain substituents extending on each side. The subsequent self-assembly of these 2D building blocks in the third dimension via complementary stacking appears to complete the formation of sandwiched bimolecular chain assemblies.

1. Introduction

Pillared, layered organic–inorganic (O/I) materials¹ have been a subject of great attention because of their extraordinary ability to combine synergistically the properties unique to purely organic or inorganic materials. Sustained interest in these materials can be attributed, in general, to the vast array of possibilities they offer in tailoring material properties simply by the correct selection of functionalized organics and variously coordinating inorganic precursors.² Extensive research over several decades has led to many classes of such molecularly hybrid materials (typically mesoscale) with a molecular level control over structure and properties.³ In particular, materials that allow systematic variations in nonlinear optical behavior,⁴ electrical conductivity,⁵ superconductivity,⁶ and ferromagnetism⁷ have been successfully prepared. Further, layered O/I materials have been constructed that exhibit controlled nanoporosities⁸ with a host of applications in sensors⁹ and catalysis.¹⁰ The majority of these layered O/I materials are prepared by selective intercalation of organic moieties into a layered, inorganic host.¹ Examples of this type include classes of materials obtained by intercalation of ionic organic/polymeric molecules through

specific electrostatic or ionic interactions into layered host-lattices of clays and silicates, double hydroxides, and metal phosphates and phosphonates.¹¹ The host surfaces provide a robust template which guides the assembly of the organics without undergoing substantial reconstruction in their native structure.¹² Despite the general success of these approaches, precise control over the assembly of the organic components in terms of orientation, density, packing, interpenetration, and stability is often difficult to achieve. This is due to the unpredictable influences of many experimental variables, including kinetics, contaminants, and competing dispersive interactions at the inorganic template.

A rational alternative, in this regard, is to explore preparative routes which allow *cooperative assembly* of the organic and inorganic precursors to form molecularly hybrid, organic–inorganic heterostructures.¹³ Examples of such co-assemblies are common in natural systems^{3c} and in solid-state crystal engineering², but the examples of formation of O/I layered motifs by this approach are rare. In this vein, layered, organo-substituted silver thiolates formed as insoluble precipitates upon simple addition of Ag⁺ ions to a basic solution of alkanethiols (RSH), reported first in 1991 by Dance and co-workers,¹⁴ are particularly exciting. Using X-ray diffraction measurements for a series of short-chain alkyl (and aryl)-substituted silver thiolates (AgSRs), the authors suggest that the precipitates formed are stoichiometrically uniform, nonmolecular sheet compounds of

* Corresponding authors. E-mail addresses: parikh@lanl.gov, basil@lanl.gov.

† Advanced Instrumentation & Diagnostics Group, CST-1.

‡ Condensed Matter and Statistical Physics Group, T-11.

§ Electrochemical Science & Devices Group, MST-11.

|| Participants, Summer Research Program, LANL.

AgSRs structured in a periodically layered arrangement of bi-molecular assemblies and the Ag–S inorganic core—reminiscent of hybrid O/I intercalated compounds. A distinguishing feature of these AgSRs is the spontaneous organization of the organic and inorganic phases simultaneously in molecularly defined periodic blocks.

While the details of the ordering in the Ag–S inorganic backbone structure appear to be well-understood, a satisfactory *direct* characterization (e.g., spectroscopic) of the organic phase is lacking. In the original paper, Dance and co-workers¹⁴ advanced the general structure of chain-substituted ($\text{AgSC}_n\text{H}_{2n+1}$, $n = 3, 4, 6,$ and 8) silver thiolates to be comprised of a uniformly layered, inorganic Ag–S lattice ($\sim 1.0\text{--}1.5$ Å in thickness) in a distorted-hexagonal symmetry extending the substituents on either side in an assembly of perpendicularly oriented all-trans ordered aliphatic chains. However, no direct experimental evidence was given for the assumptions of (1) perpendicular orientation, (2) all-trans conformational order, and (3) any interdigitation caused by the overlap of undulating van der Waals surfaces of end-methyl groups. This was correctly pointed out quite recently by Fijolek and co-workers.¹⁵ The latter authors, on the basis of their structural investigations of variously synthesized silver butanethiolates, show that chain structure in silver butanethiolates varies from an entirely all-trans to a conformationally mixed phase and a gauche phase (C–C bond adjacent to S) depending on exact synthetic conditions. This conformational disordering must influence the chain-tilting, molecular packing, and nature of interdigitation. We further note that, to the best of our knowledge, all previous structural studies of AgSRs have exclusively focused on short-chain analogues—with highly limited conformational and orientational degrees of freedom. In view of the above, a detailed spectroscopic study that examines the local molecular structure of the organic chain phase, especially for long-chain substituted silver thiolates with broad conformational flexibility, will be relevant.

In this paper, we report a joint Fourier transform infrared (FTIR) spectroscopic and X-ray diffraction (XRD) characterization of the structures of a self-consistent series of long-chain homologues of AgSRs. ($\text{CH}_3(\text{CH}_2)_n\text{SH}$, $n = 5, 6, 9, 11, 15,$ and 17). FTIR data reported in the present study are the first for any silver thiolates, and the X-ray diffraction data are first for the long-chain analogues. Because FTIR spectroscopy is a highly sensitive probe of the local molecular structure of the aliphatic chains allowing for a detailed characterization of average chain-conformational properties and packing arrangement, it provides a valuable probe with which to explore the chain structural characteristics. An analysis of interlayer structure using XRD data, together with the spectroscopic results, provides a more comprehensive characterization of chain-molecular assemblies.

Results presented here establish the bi-molecular organic phase in a set of long-chain silver thiolates ($\text{CH}_3(\text{CH}_2)_n\text{SH}$, $n = 5, 6, 9, 11, 15,$ and 17) to be comprised of assemblies of chains that exhibit (1) conformationally all-trans order, (2) perpendicular untilted orientation with respect to the inorganic Ag–S slab, (3) slight, but nonvanishing, overlap between the hydrogen atoms of methyl groups of the contiguous layers, and (4) the formation of layer-by-layer alternating (bidiscontinuous) 1D channels or voids in chain matrixes. A schematic depiction of these features is shown in Figure 1. These conclusions substantiate the assumptions made by Dance and co-workers in their X-ray determination of the intralayer Ag–S slab structure. Furthermore, all the results of the present study point to a uniform structure of the organic phase wherein the essential

chain organization is determined by the coordination geometry of the Ag–S inorganic sheet and long-range $\text{CH}_3\text{--CH}_3$ interactions and appears not to be dictated entirely by van der Waals interactions between the chains. Finally, the results presented here allow us to propose a two-step, hierarchical self-assembly mechanism involving primary self-assembly of the inorganic core to produce quasi-2D modules which subsequently self-assemble in the third dimension to produce the pillared O/I silver thiolates.

2. Experimental Section

All *n*-alkanethiols ($\text{CH}_3(\text{CH}_2)_n\text{SH}$, $n = 5, 6, 9, 11, 15,$ and 17 ; >97% purity) were obtained from Aldrich (Milwaukee, WI) and used without further purification. Water was deionized (>18 MΩ-cm resistivity) and scrubbed of organic contaminants in a Milli-RO, milli-Q purification system (Millipore, Bedford, MA). AgNO_3 was obtained from (Bio-Analytical Systems, Inc., W. Lafayette, IN). Triethylamine (99.5%) was obtained from Fluka Chemical Co. All other solvents were HPLC grade quality from Aldrich and used as received. Glassware used was cleaned prior to each use with NoChromix (Aldrich) solution in concentrated sulfuric acid (Baker Analyzed Acids), washed thoroughly with copious amounts of deionized water, and dried in a glassware oven maintained at ~ 150 °C.

Many of the details of sample preparation and characterization have been published elsewhere;^{14,16} a brief summary is provided here. To an equimolar mixture of an *n*-alkanethiol (4 mM) and triethylamine (4 mM) in acetonitrile was added silver nitrate solution (4 mM), also in acetonitrile, in a dropwise manner at a constant rate of addition (0.3–0.5 mL/min). The solution mixture was held under constant stirring at room temperature during the reaction period (12–15 h). Exposure to laboratory light was minimized by maintaining all reaction vessels wrapped with several layers of aluminum foil. Upon the formation of $\text{CH}_3(\text{CH}_2)_n\text{SAg}$, the solution turned highly turbid in all cases. After standing for 4–6 h, the precipitate was collected by suction filtration, repeatedly washed with acetonitrile, and then dried for several days under vacuum at room temperature. The collected powder was stored in a dry atmosphere until use. The color of precipitates varied between preparations, but always carried a shade between opaque brown and bright yellow. In our hands, dried compounds of long-chain silver thiolates were never white.¹⁷ The compounds appeared highly insoluble in all typical organic solvents including hexane, ethanol, tetrahydrofuran, ether, acetone, toluene, trichlorobenzene, and carbon tetrachloride up to the boiling point, with the exception of hot toluene which appeared to dissolve all compounds, though sparingly, upon vigorous stirring for several hours. The density of all the compounds, determined by immersion in different density liquids (sink-and-float method), was found to be in a narrow range of 0.86–0.88 g/cm³. Elemental analyses (Galbraith Laboratory) (average of 2 samples for each compound, all constant within 1–2 wt %) of selected compounds gave the following values: (1) $n = 15$: (obs.) C, 52.41; H, 9.19; S, 8.93; Ag, 28.58% compared to the calcd values: C, 52.60; H, 9.04; S, 8.76; Ag, 29.58%. (2) $n = 11$: (obs.) C, 45.73; H, 8.08; S, 10.47; Ag, 37.35% compared to the calcd values: C, 46.60; H, 8.09; S, 10.35; Ag, 34.95%. (3) $n = 9$: (obs.) C, 41.49; H, 7.47; S, 11.58; Ag, 36.22% compared to the calcd values: C, 42.7; H, 7.47; S, 11.38; Ag, 38.43%.

Infrared transmission spectra were obtained using a Fourier transform spectrophotometer (Bruker Optics, Göttingen, Germany) operating at 2 cm⁻¹ resolution with an unpolarized beam striking the sample at normal incidence. The beam diameter

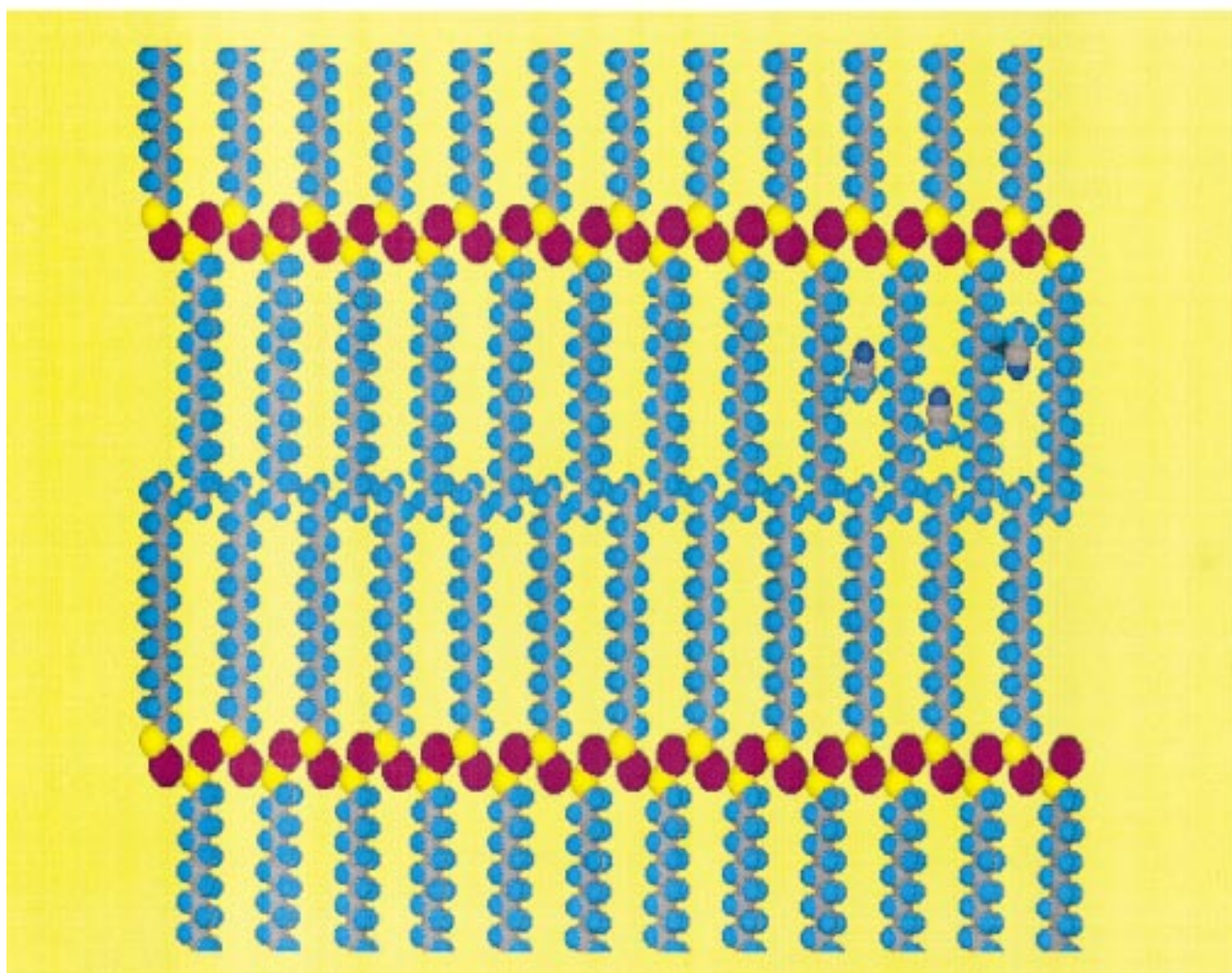
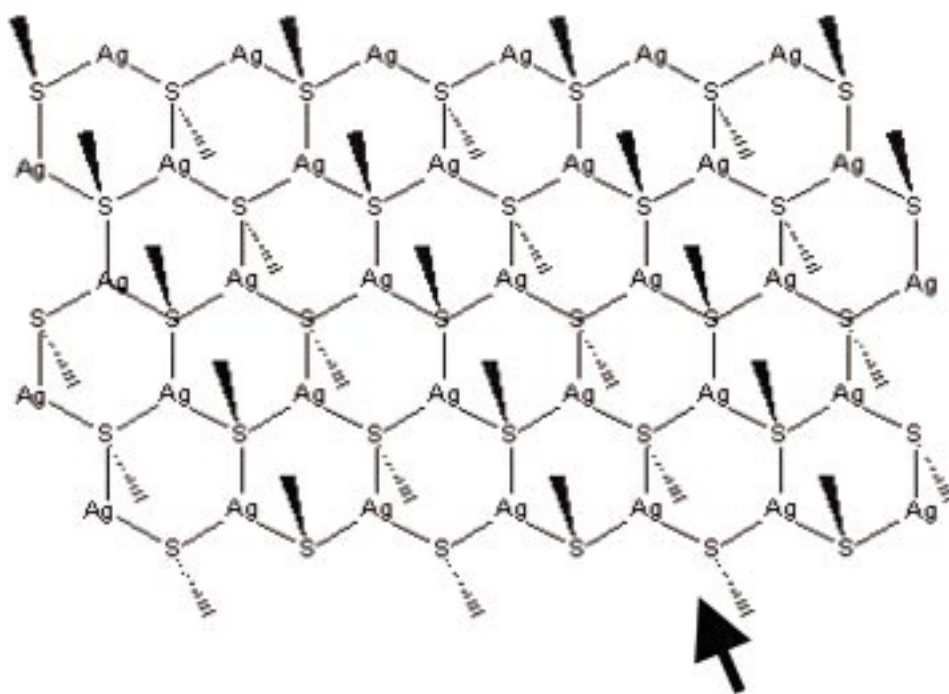


Figure 1. Model description of the proposed structure of long-chain silver thiolates. The top panel indicates the trigonal coordination of Ag with S atoms resulting in a quasi-hexagonal inorganic core of ~ 1 Å thickness. The bottom panel schematically depicts the chain orientation, packing, void, and slight interdigitation between the methyl groups when viewed along the direction indicated by the arrow.

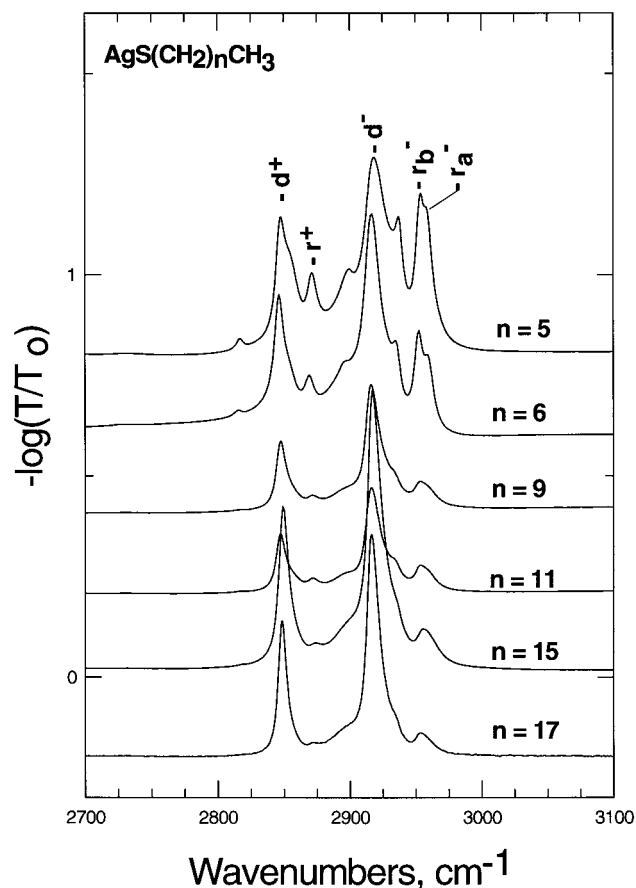


Figure 2. Infrared spectra of silver thiolates ($\text{AgS}(\text{CH}_2)_n\text{CH}_3$, $n = 5, 6, 9, 11, 15,$ and 17) in the high-frequency ($2700\text{--}3100\text{ cm}^{-1}$) region showing overlapping contributions from CH_2 and CH_3 C–H stretching modes.

was controlled at 8 mm by an aperture placed adjacent to the sample. The resulting interferograms, obtained by co-adding between 50 and 100 scans, were Fourier transformed with triangular apodization and zero-filling to increase the point density by a factor of 4 for accurate determination of peak positions. The sample consisted of essentially transparent pellets prepared by pressing a mechanically homogenized mixture of the dried solid with nominally dehydrated pure KBr in calculated quantities. The spectra were referenced against the spectra obtained for air or blank KBr pellets under identical spectrometer conditions and geometry. All spectra are reported in the transmission absorbance units, $[A = -\log(T/T_0)]$, where T and T_0 are the emission power spectra of each sample and reference, respectively. For accurately resolving overlapping peaks and precise determination of peak positions, second-derivative $[-d^2(A)/d\nu^2, \nu = \text{wavenumbers}]$ spectra are also reported. The data analysis was performed using Grams 32 (SpectraCalc) software for peak-fitting and analyses.

X-ray diffraction patterns were obtained on a Rigaku Geigerflex diffractometer (with $\text{Dmax-}\beta$ controller and a vertical goniometer) using $\text{Cu K}\alpha$ (1.541871 \AA) radiation and a graphite monochromator. The samples were prepared by packing $\sim 5\text{ mg}$ of solid in a standard cavity mount. Digital data were obtained for a 2θ range of 5° to 70° at an angular resolution of 0.02° with a total counting time of 2 h.

3. Results

Infrared Spectroscopy. Extensive studies of infrared spectra of various phases of n -alkanes over several decades have led to

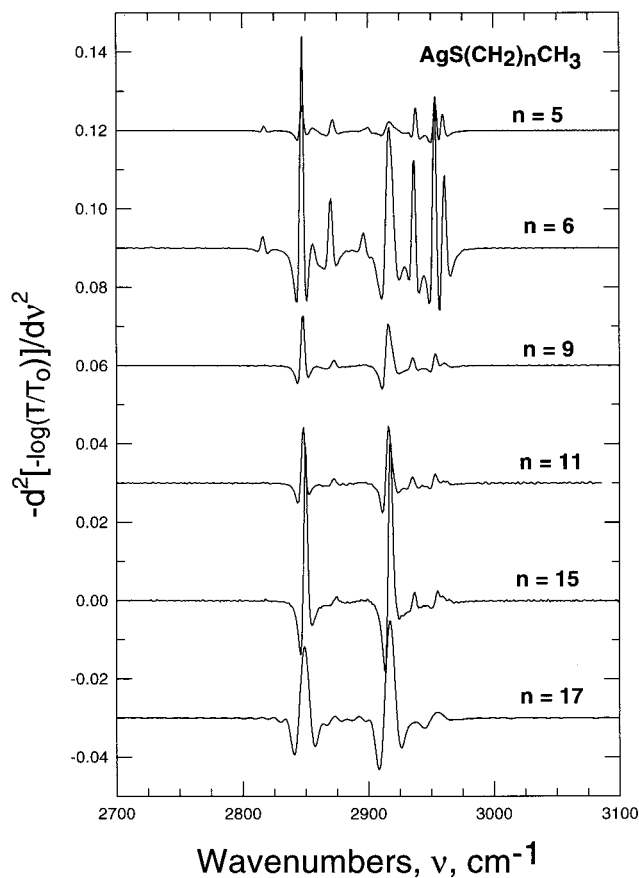


Figure 3. Second-derivative infrared spectra of silver thiolates ($\text{AgS}(\text{CH}_2)_n\text{CH}_3$, $n = 5, 6, 9, 11, 15,$ and 17) in the high-frequency ($2700\text{--}3100\text{ cm}^{-1}$) region comparing the changes in the fine structures of the contributing stretching modes.

detailed correlations between infrared spectra and such structural attributes of polymethylene $[-(\text{CH}_2)_n-]$ sequences as chain conformation, defects, and packing arrangements. These studies provide a firm basis for the extension of the vibrational analysis to related classes of chain assemblies including the organic–inorganic materials of concern here. For the purposes of convenience in presenting the spectra, we have divided the spectral region into a high- and a low-frequency region, each of which is discussed in turn below.

High-Frequency Region ($2700\text{--}3100\text{ cm}^{-1}$). Figures 2 and 3 show absorbance and second-derivative spectra in the high-frequency region for the series $\text{AgS}(\text{CH}_2)_n\text{CH}_3$, where $n = 5, 6, 9, 11, 15,$ and 17 . The characteristic band-signature of overlapping peaks observed in the absorbance spectra is straightforwardly assigned to the C–H stretching modes of the polymethylene $[-(\text{CH}_2)_n-]$ sequence and end-methyl $[-\text{CH}_3]$ groups in comparison with the previous assignments of long-chain n -alkanes.^{18,19} For more detailed assignments, peak positions of component peaks were deduced from the second derivative spectra, which revealed the fine structure of the spectral signature in remarkable detail. A summary of these assignments is given in Table 1. The asymmetric band in Figure 3 at $\sim 2954\text{ cm}^{-1}$ is assigned to the asymmetric stretching vibrations of the $-\text{CH}_3$ group (r^- modes). The derivative spectra in Figure 3 reveal that the band is actually composed of three overlapping peaks with maxima at $2954, 2959,$ and 2964 cm^{-1} . It has been well-established that for the two asymmetric stretching vibrations of a CH_3 group to become degenerate and appear as a single broad peak, the CH_3 group must be in at least C_3 symmetry. But this symmetry is lifted in the present

TABLE 1: Identification and Assignment of C–H Stretching Modes to the Observed Infrared Peak Maxima in Wavenumbers, cm^{-1} for the Series of Long-Chain Silver Thiolates, $\text{AgS}(\text{CH}_2)_n\text{CH}_3$, $n = 17, 15, 11, 9, 6$, and 5^b

n vibrational modes ^a	17	15	11	9	6	5
asym CH_3 str (op); r_a^-		2964	2962.8	2960.7	2960.9	2959.6
asym CH_3 str (ip); r_b^-		2959 (vw, sh)	2959.2		2953.2	2945.1
asym CH_3 str (ip); r_b^-	2955.1	2955 (vw, sh)	2953.3	2953.7	2944.6	2953.8
sym CH_3 str (FR); r^+ (fr)	2937.7	2937	2935.3	2935.7	2936.7	2937.9
antisym CH_2 str (op); d_a^-		2926 (vw, sh)	2928.1	2929.5 (vw, sh)	2929.2	2933
antisym CH_2 str (op); d^-	2917.3	2917	2916.3	2916.3	2916.7	2916.9
sym CH_3 str (ip); r^+	2874.1	2874	2872.5	2872.8	2870.3	2871.8
sym CH_2 str (ip); d_a^+	2864.1	2861	2860.8	2859.0	2855.9	2855.0
sym CH_2 str (ip); d^+	2849.2	2849	2848.2	2848.0	2847.3	2847.5

^a Str, stretching; w, weak; vw, very weak; sh, shoulder; sym, symmetric; FR, Fermi resonance; op, out-of-plane; ip, in-plane. ^b See text for details.

case due to the covalently attached polymethylene chain. As a result, the two asymmetric vibrations are no longer equivalent and consequently are split into at least two distinct peaks (r_a^- and r_b^- modes at 2953 and 2964 cm^{-1} , respectively) by intramolecular interactions with the polymethylene chain and by the interaction with surrounding molecules.²⁰ However, this splitting is experimentally observable only at low temperatures in what is termed the motionally narrowed limit.²⁰ Since the absorbance spectra in Figure 2 do not show the splitting, we conclude that the CH_3 groups are undergoing hindered rotation and twisting about their long axis in a motionally collapsed limit. In the latter limit, the large line widths of the individual components preclude direct observation of the splitting. The weak peak observed at $\sim 2874 \text{ cm}^{-1}$ (r^+) and a shoulder at 2937 cm^{-1} (r_{FR}^+) (appear as distinct, well-resolved peaks in the derivative spectra) are assigned to the CH_3 group's symmetric CH stretching modes. This doublet of the symmetric stretch of the CH_3 group is understood to arise from the intramolecular Fermi resonance interaction with the overtone of the CH_3 group asymmetric deformation (δ).^{19,21} Finally, the two strongest bands in Figure 2 with peak maxima at 2847–2849 and 2916–2917 cm^{-1} are assigned to CH_2 C–H symmetric (d^+) and antisymmetric (d^-) stretching modes, respectively. Derivative spectra reveal additional peaks at 2861 and 2927 cm^{-1} . We assign these contributions tentatively to the symmetric (d_a^+) and antisymmetric (d_a^-) stretchings of $\alpha\text{-CH}_2$ groups closest to the headgroups.²²

These data yield two immediate conclusions. First, the exact location of methylene symmetric (d^+) and antisymmetric (d^-) peaks is known to be a strong indicator of chain conformation. For crystalline n -alkanes, d^+ and d^- modes occur in the ranges of 2846–2849 and 2916–2918 cm^{-1} , respectively.²² These ranges are known to shift with increase in gauche population in the polymethylene ensemble and assume the ranges of 2854–2856 and 2924–2928 cm^{-1} for high-temperature disordered or liquid phases of n -alkanes.²³ In this regard, the observed positions in a narrow range of 2848–2849 and 2916–2917 cm^{-1} for all AgSRs examined here strongly indicate that the dominant structure of the polymethylene sequences in the AgSRs is all-trans comparable to that found in crystalline n -alkanes. The narrow line widths observed for the CH_2 stretching mode features, viz., $\sim 7\text{--}9 \text{ cm}^{-1}$ for d^+ modes and $\sim 10\text{--}12 \text{ cm}^{-1}$ for d^- modes for AgSRs, are in the ranges of 6–9 and 8–11 cm^{-1} reported for comparable chain-length crystalline n -alkanes²⁴ and alkane–urea clathrate compounds²⁵ – further suggesting the uniformity of the all-trans chain structure. Second, we note that for the entire series of AgSR compounds examined here, all the peaks and the fine structure appear consistently and show comparable band characteristics (peak positions, peak widths, and relative intensities) suggesting that the essential

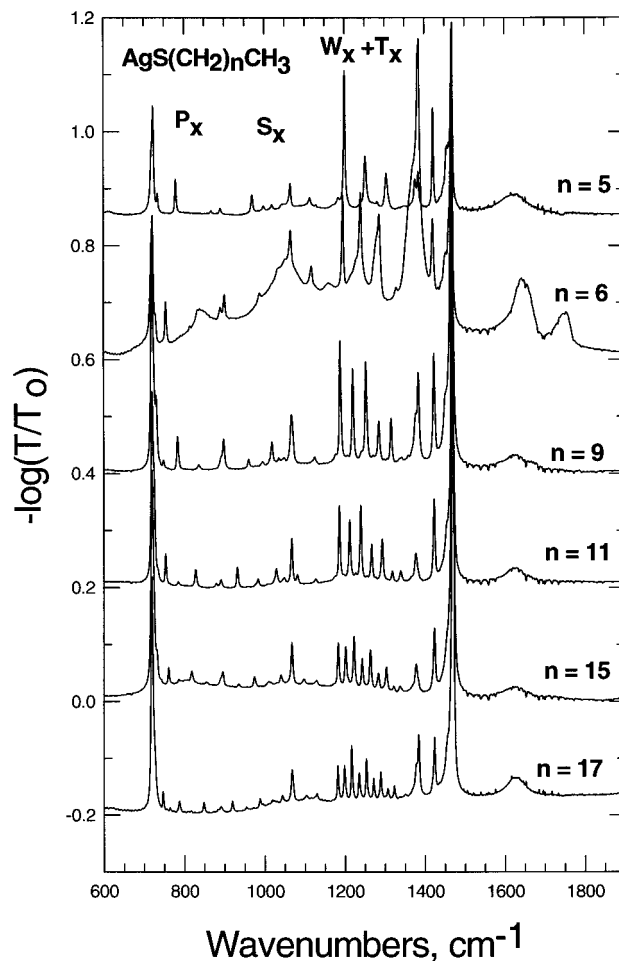


Figure 4. Infrared spectra of silver thiolates ($\text{AgS}(\text{CH}_2)_n\text{CH}_3$, $n = 5, 6, 9, 11, 15$, and 17) in the lower-frequency ($700\text{--}1800 \text{ cm}^{-1}$) region showing the prominent progression series from delocalized rocking, C–C–C skeletal stretches, wagging, twisting, and bending modes from $-\text{CH}_2-$ sequences as well as other local contributions. (See text for details.)

chain conformation is preserved across the series of compounds independent of the R group chain length.

Low-Frequency Region ($600\text{--}1800 \text{ cm}^{-1}$). Absorbance and second-derivative spectra for the series of long-chain AgSRs in the $600\text{--}1800 \text{ cm}^{-1}$ region are shown in Figures 4 and 5, respectively. Previous studies of spectra–structure correlations in n -alkanes provide an unequivocal assignment of all the prominent bands that constitute the rich spectral signatures in this region.^{18,27,28} A summary of these assignments is provided in Table 2.

The strongest band observed at $1468\text{--}1470 \text{ cm}^{-1}$ is probably the most widely used diagnostic feature of the aliphatic chain

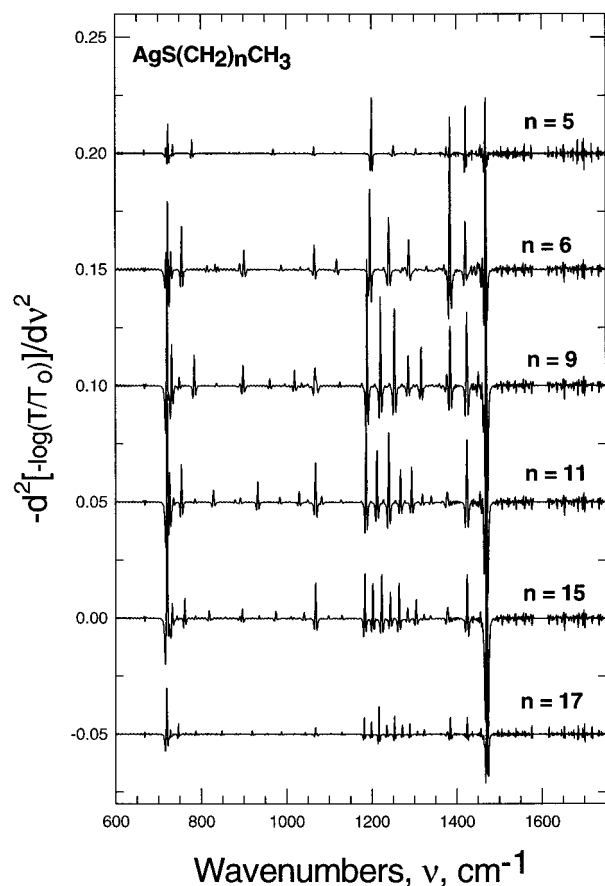


Figure 5. Second-derivative infrared spectra of silver thiolates ($\text{AgS}(\text{CH}_2)_n\text{CH}_3$, $n = 5, 6, 9, 11, 15,$ and 17) in the lower-frequency ($600\text{--}1750\text{ cm}^{-1}$) limit showing overlapping and shoulder peaks.

assemblies.²⁶ The peak appears asymmetric with a weak but reproducible shoulder at $\sim 1455\text{ cm}^{-1}$ in all spectra. As is evident in the second derivative spectra (Figure 5), the band is in fact an envelope encompassing contributions from distinct absorptions with peak maxima at $1470, 1460,$ and 1455 cm^{-1} . The 1455 cm^{-1} shoulder is assigned to out-of-plane CH_3 asymmetric deformation or bending mode (α_{op}) while the contribution at 1460 cm^{-1} is assigned to in-plane CH_3 asymmetric deformation (α_{ip}). The sharp and the strongest contributor in this region at $\sim 1470\text{ cm}^{-1}$ is assigned to the singlet due to CH_2 deformation or scissoring peak (δ).

Exact characteristics of the CH_2 deformation peak above provide a sensitive measure of the packing arrangement of the alkyl chains. In orthorhombic arrangements of the polymethylene chains, the scissoring peak is split into two components (~ 1463 and $\sim 1473\text{ cm}^{-1}$ for crystalline n -alkanes) by interchain interactions between the contiguous CH_2 groups of the two chains that constitute the crystal sub-cell.²⁷ This splitting, referred to as factor-group splitting, is specific to orthorhombic sub-cells. It is not observed in the alternative single-chain sub-cells of monoclinic, or triclinic packing, where only one peak is observed.²⁸ The observed singlet for all AgSRs at $\sim 1470\text{ cm}^{-1}$ in this regard implies that the unit cell is composed of only one chain. Taken alone, the observation above excludes the orthorhombic arrangement, but does not distinguish between the monoclinic or triclinic types of packing that may occur in polymethylene chains. However, these data in conjunction with the monoclinic structure evident for the packing of S atoms in XRD data (analyzed later in the manuscript) and the foregoing conclusion that the chains do not possess any noticeable amount of gauche conformers, suggests that the most likely packing is

the compliant pseudo-monoclinic superlattice structure for all AgSRs examined here.

The moderate and distinct peak at $\sim 1424\text{ cm}^{-1}$ observed for all silver thiolates here is intriguing and its assignment is complex. The peak is typically not observed in most n -alkanes. In a few instances, where a peak in this frequency range is observed, it has been assigned either to an overtone of a low-frequency rocking mode at $\sim 720\text{ cm}^{-1}$ or to a mixed mode arising from a coupling between CH_3 and CH_2 asymmetric deformation (α and δ) modes. Due to lack of adequate assignment for this peak, no structural interpretations are made. The peak appearing at $\sim 1377\text{ cm}^{-1}$ for all AgSRs is assigned with a high degree of certainty to the CH_3 symmetric deformation or bending (U) vibration. This mode is sensitive to the environment and to interlamellar interactions both in terms of its precise location and its bandwidth.²⁹ Its essential invariance across the series of AgSRs examined here is consistent with the uniform, chain-length-independent interlayer structure in the compounds.

Next the appearance of the series of uniformly spaced peaks of moderate intensities with alternating weak shoulders between 1175 and 1300 cm^{-1} is assigned to the progression series formed by the delocalized wagging (W_x) and twisting (T_x) vibrations of the polymethylene sequences.³⁰ The weaker series that appears as a shoulder to the more intense W_x series, revealed more distinctly in the second-derivative spectra in Figure 5, is accordingly assigned to the progression series due to T_x modes of the chain.

Salient features of these series provide important clues regarding the conformational sequence of the average alkyl chain. First, the very occurrence of the wag-twist progression series, as an exclusive property of trans-ordered segments, establishes unambiguously that the *trans* polymethylene sequence constitutes the dominant population of chain conformers in the crystals. In contrast, if the chains were disordered, as in high-temperature or liquid-phase n -alkanes, these features would diminish in intensity, broaden, and appear as long-wavelength bumps in the spectra. Additionally, the number, the intensity, and the inter-band separation all depend on the average number of trans conformers in the chains. For example, in the case of a terminally substituted alkyl chain, $\text{CH}_3(\text{CH}_2)_n\text{X}$, the inter-band spacing $\Delta\nu$ in W_x modes below $\sim 1350\text{ cm}^{-1}$ is related to m , the number of trans-units in conformational registry, and therefore the average number of methylene bonds in the trans sequence by the following equation:³¹

$$\Delta\nu = \frac{326}{m + 1} \quad (1)$$

The measured average values of $\Delta\nu$ for the $\text{AgS}(\text{CH}_2)_n\text{CH}_3$ compounds from the infrared spectra in Figures 4 and 5 are given below: $\Delta\nu = 18.4, n = 17$; $\Delta\nu = 20.5, n = 15$; $\Delta\nu = 27.2, n = 11$; $\Delta\nu = 31.8, n = 9$; $\Delta\nu = 46.3, n = 6$; and $\Delta\nu = 56.2, n = 6$. Using eq 1, we derive the average trans segment length, m , in terms of number of methylene units to be $m = 16.7, n = 17$; $m = 14.9, n = 15$; $m = 10.98, n = 11$; $m = 9.25, n = 9$; and $m = 4.8, n = 5$. These numbers show remarkably well, that within the errors of the frequency estimations, nearly the entire length of the chain substituent is in all-trans conformation with gauche defect concentration for an average chain to be within $\pm 0.4\%$, an uncertainty well within the experimental inaccuracies imposed by the resolution limit in our data.

Another relevant feature of interest in this region of the spectra of polymethylene assemblies, in general, is the presence

TABLE 2: Identification and Fundamental Vibrational Assignment of Low-Frequency Modes (720–1800 cm⁻¹) to the Observed Infrared Peak Maxima in Wavenumbers, cm⁻¹ for the Series of Long-Chain Silver Thiolates, AgS(CH₂)_nCH₃, n = 17, 15, 11, 9, 6, and 5^b

<i>n</i> vibrational modes ^a	17	15	11	9	6	5
CH ₂ rock; P ₁	719.52	720.71	720.73	720.74	719.01	719.11
P ₃	728.13	732.82	735.58	731.51	722.7	723.58
P ₇	746.71	761.51	754.28	749.15	730.09	734.85
P ₉	762.52	786.35	785.52	784.32	744.45	779.59
P ₁₁	787.32	818.99	828.83	837.02	755.51	868.42
P ₁₃	848.31	855.44	879.58		833.94	
P _{CH₃}	891.14	896.42	891.84	898.33	891.38	890.75
					901.33	
P _X	919.44	933.53	932.76	961.72	988.02	969.97
P _X	953.16	975.01	983.83	995.03	1066.3	999.06
P _X	988.21	1009.8	1029.6	1019.1	1118.7	1019.7
C–C–C skeletal; S _x	1041.2	1041.1	1050	1035.1	1161.1	1065.4
S _x	1067.8	1068.6	1068.1	1048.7		1114.4
S _x	1129.9	1098.7	1082.5	1067.1		1129.9
S _x		1130.4	1128.5	1124.5		1185.4
S _x			1177	1177.1		
CH ₂ Wag; W _x	1182.3	1183.9	1187.1	1189.6	1197.1	1200.8
CH ₂ Twist; T _x	1192.8	1193.4	1198.4	1207.4	1229.7	1241.6
W _x	1198.9	1202.8	1212.7	1221.1	1241.3	1252.4
T _x	1209.9	1209.7	1227.9	1242.1	1288.3	1282.7
W _x	1217.0	1223.5	1240.5	1254	1329.4	1305.2
T _x	1229.1	1232.2	1255.9	1271.5		
W _x	1235.5	1243.9	1267.7	1286		
T _x	1241.9	1252.8	1278.2	1306.3		
W _x	1253.7	1264.6	1294.4	1315.8		
T _x	1265.5	1275.4	1308.9	1341.4		
W _x	1271.9	1284.7	1319.5	1359.3		
T _x	1283.6	1296.7	1340.2			
W _x	1289.5	1304.4				
T _x	1307.2	1323.5				
W _x	1323.4	1338.9				
CH ₃ sym def, bend, U	1377.7	1378.7	1377.7	1377.2	1370.9	1376.5
	1384.6			1385.1	1385	1384.8
α + δ, ?	1424.4	1424.7	1424	1424.2	1421.2	1421.6
CH ₃ asym def, op, α _{op}	1456.7		1454.8		1450.5	1456.6
CH ₃ asym def, ip, α _{ip}	1459.6	1460.1	1459.4	1460	1459	1458
CH ₂ def, scissor, δ	1470.4	1470.3	1469.9	1469.5	1468.3	1468.3

^a def, deformation; sym, symmetric; op, out-of-plane; ip, in-plane. ^b See text for details.

(or absence) of peaks exclusive to localized vibrations of nonplanar or gauche conformations. For example, the spectral region between 1300 and 1375 cm⁻¹ contains bands exclusively due to defects or nonplanar conformers.³² In particular, the presence of end-gauche defects (*gt_m*) is known to result in a peak at ~1341 cm⁻¹, whereas internal kink defects formed by *gtg'* sequences between two all-trans segments are known to yield new broad peaks at 1306 and 1366 cm⁻¹. The fact that we find no evidence for the existence of these peaks for any of the AgSRs examined here further corroborates (but does not independently establish) the inference above: the aliphatic chain substituents adopt a largely defect-free, all-trans conformational habit in long-chain AgSRs.³³

At even lower frequencies, two additional sets of peak series are evident. The series of peaks observed for all silver thiolates between 1000 and 1150 cm⁻¹ are assigned to the degenerate progression due to skeletal C–C–C vibrational modes (S_x) whereas the second set of bands observed between 720 and 980 cm⁻¹ is assigned to the rocking modes (P_x) of the chain methylenes. All the peaks, except one, in this spectral region are chain-delocalized. The exception is the chain-length-independent peak observed at ~890 cm⁻¹ which is assigned to the local rocking motion of the CH₃ group. The structural implications of the S_x series of modes between 1030 and 1130 cm⁻¹ are difficult to decipher, and such analyses will not be attempted here.

The most intense asymmetric band observed at ~720 cm⁻¹ is assigned to the head-band (P₁) of the progression series of the P, or rocking, modes. In close analogy to the CH₂ scissoring mode at ~1467 cm⁻¹, this band is also known to show packing-dependent features. Orthorhombic packing is known to split the P₁ mode into two components of comparable intensities by factor-group splitting, but the vibrational levels are not split when the packing is monoclinic, triclinic, or hexagonal containing only one chain per sub-cell. The observed spectra in Figure 4 show only one sharp and strong band at ~719 cm⁻¹ with a fine structure on the higher-frequency side. Since the intensity of the high-frequency shoulder is significantly lower than the principal band at 719 cm⁻¹, we reliably conclude that the weaker band at ~732 cm⁻¹ is the higher-order peak from the progression series rather than the split-component of the head-band. This assignment is directly supported by the singlet observed for the CH₂ scissoring band earlier. The packing structure then must include single chain per sub-cell. The sharpness of the peaks however precludes hexagonal arrangement and the most likely packing inferred from the above considerations is therefore monoclinic or triclinic. The XRD data further allow us to resolve the two packing arrangements. The unit-cell description derived from the XRD data (see below) suggests the most likely chain-packing to be distorted monoclinic.

X-ray Diffraction. Powder XRD data³⁴ provide quantitative descriptions of inter- and intralayer structures in organic–

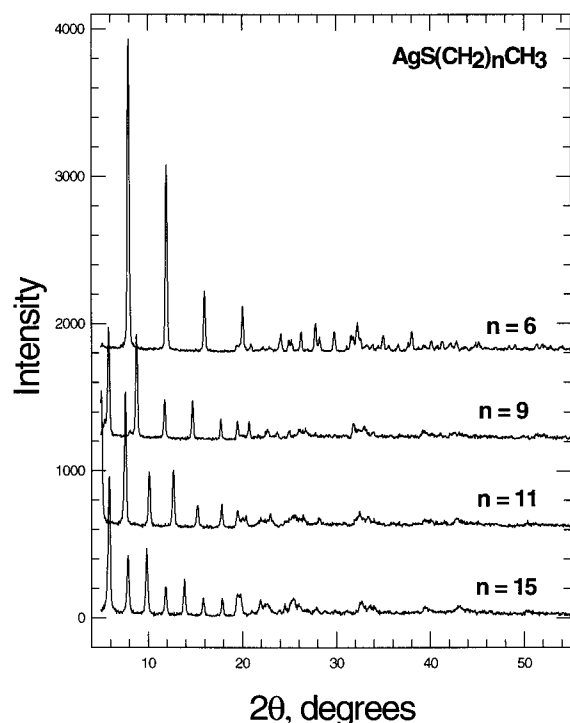


Figure 6. Powder X-ray diffraction data for selected long-chain silver thiolates ($\text{AgS}(\text{CH}_2)_n\text{CH}_3$, $n = 6, 9, 11,$ and 15).

inorganic layered compounds. The intralayer structure provides the packing characteristics of the organic as well as the inorganic slabs while the interlayer structural attributes provide characterization of the uniformity and the layer thicknesses. The interlayer structural analysis presented here extends previous studies of short alkyl chain derivatized $\text{CH}_3(\text{CH}_2)_n\text{SAg}$ ($n = 3, 5,$ and 7) by Dance and co-workers¹⁴ where the characterization of the structure of Ag-S inorganic slab was the main focus. Since our data span a broader range of chain lengths, a new opportunity to test the validity of the assumptions of the chain orientation and interlayer overlap is afforded. Further, the FTIR spectroscopy evidence given above is used to constrain the XRD data analysis, thereby yielding a rigorous elucidation of the interlayer chain structure.

Figure 6 shows the XRD data for selected longer-chain-length silver (n -alkyl) thiolates ($\text{AgS}(\text{CH}_2)_n\text{CH}_3$, $n = 7, 9, 11,$ and 15). As for short chain AgSRs, the XRD data in Figure 6 for the long-chain derivatives shows a well-defined progression of intense reflections. A single large d spacing accounts remarkably well for all intense, well-resolved peaks ($d > 4.5 \text{ \AA}$) as successively higher orders of diffraction. The chain-length invariance of the weaker peaks, corresponding to $d < 4.5 \text{ \AA}$, confirms their assignment to the intralayer Ag-S lattice structure and periodicities. A detailed summary of the X-ray peak structure and their crystallographic assignments is provided in Table 3.

First, we discuss the interlayer structure. The d spacings evaluated for the AgSRs examined here from ($0b0$) X-ray peaks are as follows: $d = 22.20$, $n = 6$; $d = 30.1$, $n = 9$; $d = 34.8$, $n = 11$; and $d = 44.75$, $n = 15$. An informative way to interpret these long-period d data in terms of the interlayer structure of the organic phase is to plot the chain-length dependence of the estimated interlayer distances. A graphic representation of the dependence of the interlayer d spacing against $2n$, where n is the number of CH_2 units in the molecule is shown in Figure 7. Also shown in Figure 7 are previously reported values for the short-chain AgSRs. All data reveal strict monotonic dependence

TABLE 3: Summary of the Interlayer XRD Peaks and Their Assignments for Selected Long-Chain Silver Alkanethiolates, $\text{AgS}(\text{CH}_2)_n\text{CH}_3$, $n = 15, 11, 9,$ and 6

n	15	11	9	6
assignments	2θ , deg (\AA)	2θ , deg (\AA)	2θ , deg (\AA)	2θ , deg (\AA)
(010)				
(020)		5.0467	5.8201	7.9331
		(17.5107)	(15.1855)	(11.1449)
(030)	5.9018	7.5951	8.7699	11.9514
	(14.9754)	(11.6401)	(10.0832)	(7.4053)
(040)	7.8816	10.1211	11.7657	15.9864
	(11.2176)	(8.7400)	(7.5217)	(5.5441)
(050)	9.8612	12.6816	14.7080	20.0238
	(8.9697)	(6.9804)	(6.0230)	(4.4344)
(060)	11.8777	15.2573	17.7017	24.0840
	(7.4510)	(5.8073)	(5.0105)	(3.6953)
(070)	13.8676	17.8261	20.7083	28.1981
	(6.3860)	(4.9759)	(4.2894)	(3.1648)
(080)	15.8552	20.3852	23.7139	32.2353
	(5.5897)	(4.3566)	(3.7521)	(2.7770)
(090)	17.8528	22.9794	26.1283	
	(4.9685)	(3.8703)	(3.4106)	
(0100)	19.7938	25.6481		
	(4.4854)	(3.4733)		

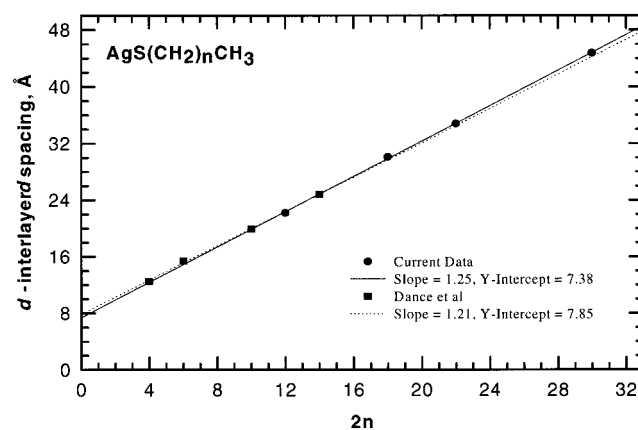


Figure 7. Dependence of the long-period, estimated from data shown in Figure 6, on the second-multiple of the number of CH_2 units. For comparison, previously determined values for the shorter-chain analogues are also shown. The legend summarizes the calculations of slope and Y -intercepts by a linear regression method.

of interlayer spacing with the number of chain methylenes. Linear regression analysis in the long-chain ($n = 6-15$) regime yields the slope of 1.25 \AA per CH_2 group and the Y -intercept of 7.38 \AA . In comparison, the previously reported data for shorter-chain thiolates provide comparable but slightly different values of slope and Y -intercept at 1.21 \AA per CH_2 group and 7.85 \AA , respectively.

To relate these values to the interlayer structure in long-chain AgSRs, we first compare the derived slope value with the corresponding estimate for an idealized model of the interlayer chain structure in the AgSR compounds. The idealized model was assumed to consist of fully extended, all-trans ordered chain in the orientation perpendicular to the inorganic Ag-S slab. Using the bond lengths and angles derived from tabulations of covalent and van der Waals radii³⁵ for the idealized model, we calculate a chain length of $1.253 (\pm 0.002) \text{ \AA}$ per CH_2 group. Using simple geometric constructions, the observed slope, m_{obs} ($= 1.25$), can be related to the incremental chain length for the idealized model to derive the average tilt angle, θ , of the chain axis from the normal to the Ag-S plane using $\theta = \cos^{-1}(m_{\text{obs}}/1.253)$. These calculations yield the average chain tilt of $0-5^\circ$. Since the assumption of all-trans order made for the idealized model is already substantiated amply in our FTIR data (dis-

cussed earlier in the manuscript), we conclude that the *average chain in the assembly is indeed oriented such that its main C–C–C backbone axis is essentially perpendicular to the inorganic backbone*. Next, we examine the structural implications of the *Y*-intercept. The experimentally derived *Y*-intercept value of 7.38 Å, corresponds to two times the thickness of the CH₃–S–Ag residue. Analyses of this value in terms of various plausible models for the Ag–S slab provide important insights into the interlayer overlap. The untilted all-trans chain orientation (determined above) makes it necessary that the S–C bond must make an angle of $\sim 35.3^\circ$ with the normal to the Ag plane. Using van der Waals radius of 2.0 Å for CH₃ group and 1.81 Å for the S–C bond-length, we obtain as a first approximation the model thickness of the 2x (CH₃–S) residue to be $2x(2.0 + 1.81 \times \cos 35.3^\circ) = 6.96$ Å. The discrepancy of 0.42 Å can therefore be understood to arise from the unaccounted contribution from the Ag–S slab thickness and the ignored overlap that may exist between the adjacent layers. Any such overlap will serve to increase the discrepancy above, and in this regard the value of 0.42 Å can be interpreted to represent the *lowest thickness contribution* from the Ag–S lattice. On this basis, it is clear that the *Ag–S lattice must be at least slightly nonplanar*. Indeed, the currently accepted model of triply bridging Ag–S lattice in primary chain substituted silver thiolates suggest that the Ag–S slab is at least ~ 1.0 Å thick with S atoms extending 0.5 Å on either side of the Ag plane.^{14,15} Incorporating this Ag–S slab thickness in our calculations, we note that the calculated thickness for the residue [$2 \times (0.5 + 1.48 + 2.0) = 7.96$ Å] now exceeds the estimated value of 7.38 Å by 0.58 Å. We interpret this difference to quantify the *extent of overlap* between the CH₃ groups of the contiguous layers in the bimolecular assembly. Clearly, any uncertainties in the presumed slab thickness for the Ag–S lattice will accordingly reflect in our estimates of the overlap.³⁶

The crystallographic registry between the bimolecular chain layers is evident from the sharpness of the strong diffraction peaks corresponding to the long interlayer period. The width of the first-order peaks (estimated from satellite peaks in our diffraction data) at ~ 0.25 – 0.30° using Scherrer's empirical equation³⁷ yields the number of translationally correlated Bragg reflection peaks in a narrow range of 270–325 Å. On the basis of the interlayer distances of each compound, this amounts to the formation of crystallites composed of 6–11 correlated bilayer stacks along the interlayer periodicity. The intralayer registry similarly calculated from the strongest intralayer peak at ~ 4.55 Å is equivalent to ~ 60 – 70 translationally correlated C–C–C planes.

While the determination of intralayer Ag–S structure is, in principle, possible from the XRD data presented here, the low signal-to-noise ratios for the peaks observed at $d < 4.5$ Å precluded any analysis from our data beyond what is previously reported using X-ray data for the short-chain analogues by Dance and co-workers.¹⁴ We, however, emphasize that the majority of the discernible peaks in this region are in good conformity with those previously reported. Further, the spectroscopic evidence presented above fully justify the assumptions in analysis presented by these authors.¹⁴ The intralayer Ag–S structure they advance is composed of an artificially symmetric, quasi-hexagonal network formed by triple coordination of Ag with three S atoms of the RS residue and RS coordinated by three Ag atoms in pseudo-tetrahedral geometry. In their model, S atoms are displaced by ~ 0.5 Å above and below the central Ag plane.³⁸ The assumption of the small but nonvanishing thickness of the S–Ag distorted plane is entirely consistent with

the analysis of the *Y*-intercept in the XRD data presented above, whereas the assumption of triple-coordination for the Ag–S is also quite reasonable given the singular long-periods inferred for all AgSR compounds. Indirect support for the triple-coordination is obtained in the fact that all the AgSR crystallites were brightly colored. Previous studies of structurally analogous silver thiolates have indicated that AgSRs with triply coordinated Ag are yellow, whereas purely two-co-ordinate species are invariably white.³⁹ The puckered sheet structure proposed above for the Ag–S core is consistent with an Ag–S bond-length of 2.56 Å with a distorted tetrahedral environment for the S atom. According to this model, the two-dimensional *ac* unit cell parameters are 4.35 Å \times 8.70 Å, $\beta = 120^\circ$. The distance of ~ 0.5 Å of S from Ag plane puts the Ag–S bond at an angle of 10.1° relative to the Ag plane. The Ag–S–Ag angle is 116.9° , whereas S–Ag–S angles are 116.9° and 121.9° . The projected in-plane Ag–S distance is 2.51 Å and the nearest neighbor distance between Ag atoms and consequently between the equivalent in-plane S atoms along the shorter dimension, *a*, is 4.35 Å. The all-trans chains are consequently spaced at the 4.35 Å along the *a* axis; a repeat distance quite comparable to the experimentally reported chain–chain separations of 4.15–4.5 Å in dense phases of crystalline *n*-alkanes. The occupancy along the longer, *b*, dimension, however, is halved with the repeat distance of 8.70 Å yielding an average surface chain density of ~ 32.77 Å²/molecule in each layer.

4. Discussion

Structural Summary. Taken together, the infrared vibrational spectroscopy and X-ray diffraction evidence presented above unambiguously establish the structure of the organic phase of long-chain silver thiolates to be composed of periodically stacked, two-dimensional bi-molecular assemblies of conformationally, orientationally, and translationally ordered alkyl chains separated by inorganic Ag–S lattices. Each chain layer incorporates periodically spaced 1D channels or corridors. This general picture is consistent with the features implied in the schematic of Figure 1. Specific details of the chain-conformation, packing, orientation, interdigitation, and void characteristics that emerge from the cumulated evidence in the present study are discussed below.

The general class of ordered structures of substituted polymethylene chains is known to form with various degrees of conformational ordering. The degree of ordering ranges from fully extended all-trans polymethylene sequences to more defective, disordered structures that incorporate isolated gauche conformal sequences in the chain interior or at the chain termini. Infrared spectroscopy data across the series of long-chain homologues of silver (*n*-alkane) thiolates (AgS(CH₂)_{*n*}CH₃, *n* = 5, 6, 9, 11, 15, and 17) examined here, consistently show the existence of uniformly all-trans conformational order with little or no detectable signal from localized defect bands. The apparent absence of localized defect peaks even in the spectra of most concentrated samples indicate that such defects, if any, in the present case of silver thiolates are in vanishing concentrations. The precise values of conformationally sensitive methylene symmetric (*d*⁺) and antisymmetric modes (*d*[−]) observed in the narrow ranges of 2847–2849 and 2916–2917 cm^{−1}, respectively, are among the lowest values reported for the densest crystalline phases of aliphatic chain assemblies of comparable molecular lengths²³ and correspond excellently with the normal coordinate predictions of these frequencies.¹⁹ The presence of well-defined wagging, twisting, and rocking mode progression series further support the conclusion of the near-exclusive

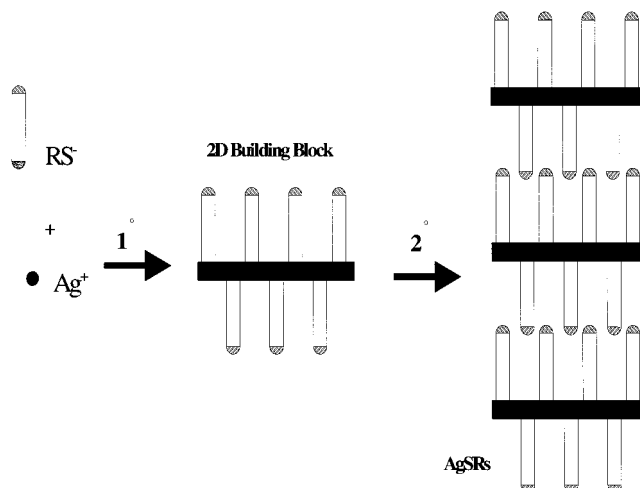
presence of the all-trans conformational order in the alkyl chains. Remarkable agreement between the estimates of all-trans sequence from wagging modes and the actual number of methylene bonds in each molecule further corroborates that, within the errors of the analysis, the entire length of the molecules is in all-trans extended sequence. Indirect support for this conclusion is also found in the estimated rate of change of interlayer long period as a function of chain length. The estimated value of 1.25 Å/CH₂ unit is consistent with the all-trans structure across the homologous series.

Next, we consider the packing arrangement of the polymethylene chains in the long-chain silver thiolates. Despite diverse structural varieties of long-chain *n*-alkanes and their end-substituted derivatives, there appear to be only four distinct ways in which polymethylene chains can be packed. Two of these, called orthorhombic and monoclinic, may be characterized by a sub-cell composed of two types of parallel polymethylene chains rotated so that their C–C–C skeleton planes make an angle a little smaller than 90° with each other.⁴⁰ In this regard, the hexagonal phase is the packing arrangement obtained from the reconstructed orthorhombic phase above the transition temperature,⁴¹ wherein the interchain separation is significantly larger and rotation of the chains about their 2-fold screw axes occurs.⁴² The triclinic phase, on the other hand, results from an entirely different kind of a sub-cell composed of two methylenes from the same chain, with chain axes and the skeleton planes of all molecules in the crystal parallel.²⁸ For all silver thiolates examined here, the lack of factor-group splitting in peaks assigned to methylene rocking (~720 cm⁻¹) and bending modes (~1469 cm⁻¹) is consistent with a unit cell composed of single type of chains in a distorted monoclinic packing.⁴³

As discussed earlier, estimation of the long period from the X-ray diffraction data provides conclusive evidence of the orientation of the chains normal to the Ag–S plane. The estimated distance of 1.25 Å per CH₂ unit from X-ray diffraction data, in conjunction with all-trans conformation of the chains established by the spectroscopic evidence, is in excellent agreement with the theoretical estimate of 1.257 Å change in thickness of the vertically oriented all-trans ordered molecule. The estimated interchain spacing of 4.35 Å based on the intralayer description indirectly supports the conclusion of perpendicular orientation of the chains.

The 3D order in the bimolecular assembly suggests that translation by *b* units allows the chains from one layer to fit into gaps created by the assembly in the contiguous layer. This, coupled with the estimated 0.58 Å interdigitation between the chains, reveals the formation of a dense lattice of undulating CH₃ groups with overlapping H atoms at the chain–chain interlayer interface. The lack of any substantial interdigitation between the polymethylene chains, coupled with the conclusions of relaxed chain occupancy along the *c* axis, all-trans order of the chains, and the perpendicular orientation indicates that 1D channels or voids are formed in the chain layers. We estimate, on the basis of the chain structure determined here, that each chain-molecular assembly contains a periodic array of channels or corridors in the space created by the uniform distribution of chain “pillars”. The channels in each chain layer are laterally displaced with respect to the adjacent layer by one molecular diameter along the larger *c* axis forming a 3D network of channels in a layer-by-layer alternating arrangement. The width of the channels is determined by the distance between the chains in each layer along the longer in-plane dimension (estimated at ~8.7 Å), less the van der Waals diameter of the chains. Their heights are similarly determined by the length of the all-trans

SCHEME 1: A Schematic Depiction of the Proposed Hierarchical Self-Assembly Mechanism for the Formation of Long-Chain Silver Thiolates^a



^a The primary self-assembly involves the organization of the molecular precursors to form a quasi-2D Ag–S lattice with the alkyl groups extending on each side. The latter 2D building blocks stack subsequently in the third dimension to generate the pillared layered AgSR structure.

extended molecule, $d/2$, less the overlap distance. The channel-width of ~4.5 Å derived from this basis suggests that they may be able to contain small solvent molecules. Thus, they may be quite useful in studies of single-molecule reactivities in confined structural environments. Our attempts to identify the presence of any intercalated solvent (acetonitrile) molecules were inconclusive. Controlled experiments to resolve this issue are currently in progress. At present, it is unclear to us why the 1D channel structure is stabilized in long-chain substituted silver thiolates as opposed to a conformationally disordered structure or a uniform chain structure because full inter-digitation of the chains between the contiguous layers appears possible. But it is possible that the activation barrier for such complete inter-digitation may be very high due to the presence of solvent molecules during the stacking assembly, slight mis-match in the crystallographic registry, incompatibly rotated C–C–C planes of the adjacent layers, as well as steric and entropic costs.

Hierarchical Self-Assembly as the Crystal Formation Mechanism. The apparent similarity of the bilayer motif represented in the class of long-chain substituted silver thiolates above and the bilayer geometry (a canonical aggregation pattern) in typical amphiphiles⁴⁴ is highly fortuitous. The chain-length independence, presence of interchain voids, and small interdigitation between the chain assemblies of the adjacent layers all suggest that the observed packing of the alkyl chains does not represent the most efficient packing of chains, rather it appears to reflect geometric constraints imposed by the integral Ag–S inorganic core. This suggests a complex formation mechanism—one in which the organization of the chains plays a secondary role. Strong coordination propensities between S⁻ and Ag⁺ further leads us to believe that the crystallization mechanism in silver thiolates must occur in hierarchical steps such as proposed below.

On the basis of results presented in this study, as well as those reported earlier for analogous layered compounds of AgSRs, we propose a two-step crystallization mechanism. A cartoon depiction of these steps is illustrated in Scheme 1. First, the primary self-assembly process, wherein the puckered quasi-2D sheets of the Ag–S lattice are formed, occurs by directed assembly of Ag⁺ ions with the –SR or deprotonated thiols. The

strong triple coordination between Ag and S appears to drive this assembly. The Ag–S sheets so formed are not entirely 2D since the alkyl R groups extend on either side of the sheets in a predisposed distribution determined by the lattice dimensions of Ag–S sheets. The pseudo-2D building blocks then stack in the third dimension via a secondary self-assembly process wherein the translationally related registry between the 2D Ag–S sheets is developed by simple van der Waals interactions between the methyl groups.

The crystallization mechanism above, if operative, will have important ramifications. First, an important ingredient in the above mechanism is the ability of the 2D motif created in situ to preserve its essential structure during the subsequent stacking process. Here, since the stacking results from weaker van der Waals interactions in comparison to the strong directional interactions between Ag and S ions in the primary self-assembly, it appears reasonable to suggest that stacking does not perturb the inorganic backbone structure. Second, by suitably choosing the organic substituents such as bifunctional chain molecules or mixtures of short and long alkanethiols, the chain density could be manipulated allowing for a formation of channels of larger and controllable widths. Alternatively, by choosing polar headgroup terminated thiols, one could conveniently alter the end-group interactions that drive the secondary stacking to further elaborate the types of structures accessed.

A Comparison with Analogous Classes of Intercalated Materials. Finally we briefly address analogies with other organic–inorganic materials. The long chain silver (*n*-alkane) thiolates in the present study belong to a large family of pillared layered systems of O/I hybrid materials¹ and bring to this family a new class of crystalline layered structures. Within this larger family, several related organic–inorganic heterolayered structures are formed by intercalation chemistry including most popularly, the surfactant–silicates and metal phosphates and phosphonates. A distinctive feature of the silver thiolates in this regard is the fact that the organic chain groups are integral or covalently tethered to the inorganic sheets in contrast to the ionic interactions that hold together organic and inorganic phases in intercalated compounds. Finally, the hierarchical self-assembly mechanism proposed for AgSRs is in remarkable analogy with that advanced for the recently reported class of pillared 2D hydrogen-bonded networks comprising guanidinium and alkanesulfonate ions,^{12,13} also formed in a two-step hierarchical self-assembly process.

Conclusions

Joint X-ray and FTIR characterization of a series of long-chain silver (*n*-alkyl) thiolates, synthesized using reaction of alkanethiols with silver nitrate from their dilute basic solution, reveal the formation of pillared layered structures composed of distinct Ag–S inorganic slabs separated by ordered bimolecular assemblies of alkyl chain substituents. The details of the chain structure and packing reveal that the bimolecular assemblies are composed of all-trans ordered alkyl chains oriented perpendicular to the Ag–S inorganic 2D lattice in an expanded, pseudo-monoclinic sub-cell. The gap along the expanded in-plane lattice and the cross-digitation between terminal CH₃ groups characterize the 1D channels formed in each chain layer. The 3D distribution of these channels is alternating between contiguous layers resulting in a bi-discontinuous array of voids. The assembly structure characteristics point to a two-step, hierarchical self-assembly mechanism for the formation of AgSR crystals.

Acknowledgment. We acknowledge the help of P. Haridoss and F. Garzon in obtaining X-ray diffraction data. Valuable discussions with T. Zawodzinski are gratefully acknowledged. This research was supported by Los Alamos National Laboratory.

References and Notes

- (1) See, for example: (a) Levy, F. *Intercalated Layered Materials*; D. Reidel: Dordrecht, The Netherlands, 1979. (b) Whittingham, M. S.; Jacobson, R. A. *Intercalation Chemistry*; Academic: New York, 1982. (c) Giannelis, E. P. *Adv. Mater.* **1996**, *8*, 26. (d) Fergusson, G. S.; Kleinfeld, E. R. *Adv. Mater.* **1995**, *7*, 414–416. (e) Alberti, G.; Marmottini, F.; Murciamascos, S.; Vivani, R. *Angew. Chem., Int. Ed. Engl.* **1994**, *33*, 15–16. (f) Alberti, G.; Casciola, M.; Costantino, U.; Vivani, R. *Adv. Mater.* **1996**, *8*, 291–303. (g) Novak, B. M. *Adv. Mater.* **1993**, *5*, 422–433.
- (2) (a) Desiraju, G. *Crystal Engineering the Design of Organic Solids*; Elsevier: New York, 1989. (b) Stein, A.; Keller, S. W.; Mallouk, T. E. *Science* **1993**, *259*, 1558–1564, and references therein.
- (3) (a) Lawrence, D. S.; Jiang, T.; Levett, M. *Chem. Rev.* **1995**, *95*, 2229–2260, and selected references therein. (b) Ozin, G. A.; Chomski, E.; Khushalani, D.; MacLachlan, M. J. *Curr. Opin. Coll. Inter. Sci.* **1998**, *3*, 181–193. (c) Ozin, G. A. *Adv. Mater.* **1992**, *4*, 612–649, and selected references therein. (d) Sellinger, A.; Weiss, P. M.; Nguyen, A.; Lu, Y. F.; Assink, R. A.; Gong, W. L.; Brinker, C. J. *Nature* **1998**, *394*, 256–260.
- (4) (a) Lacroix, P. G.; Clement, R.; Nakatani, K.; Zyss, J.; Ledoux, I. *Science* **1994**, *263*, 658–660. (b) Blanc, D.; Peyrot, P.; Sanchez, C.; Gonnet, C. *Opt. Eng.* **1998**, *37*, 1203–1207. (c) Eaton, D. F. *ACS Symp. Ser.* **1991**, *455*, 128–156. (d) Lin, W. B.; Lin, W. P.; Wong, S. K.; Marks, T. J. *J. Am. Chem. Soc.* **1996**, *118*, 8034–8042.
- (5) (a) Roth, S.; Burghard, M.; Leising, G. *Curr. Opin. Solid State Mater. Sci.* **1998**, *3*, 209–215. (b) Alberti, G.; Casciola, M. *Solid State Ionics* **1997**, *97*, 177–186. (c) Ouahab, L. *Chem. Mater.* **1997**, *9*, 1909–1926. (d) *Science* **1994**, *266*, 1013–1015.
- (6) Choy, J. H.; Kwon, S. J.; Park, G. S. *Science* **1998**, *280*, 1589–1592.
- (7) (a) Day, P. J. *Chem. Soc., Dalton Trans.* **1997**, *5*, 701–705. (b) Clement, R.; Girerd, J. J.; Morgansternbadarau, I. *Inorg. Chem.* **1980**, *19*, 2852–2854.
- (8) (a) Davis, M. E.; Saldarriaga, C.; Montes, C.; Garcés, J.; Crowder, C. *Nature* **1988**, *331*, 698–699. (b) Moore, P. B.; Shen, J. *Nature* **1983**, *306*, 356–358. (c) Pinnavaia, T. J. *Science* **1983**, *220*, 365–371. (d) Kresge, C. T.; Leonowicz, M. E.; Roth, W. J.; Vartuli, J. C.; Beck, J. S. *Nature* **1992**, *359*, 710–712.
- (9) (a) Wolf, R.; Asakawa, M.; Ashton, P. R.; Gomezlopez, M.; Hamers, C.; Menzer, S.; Parsons, I. W.; Spencer, N.; Stoddard, J. F.; Tolley, M. S.; Williams, D. J. *Angew. Chem., Int. Ed. Engl.* **1998**, *37*, 975–979. (b) Bein, T.; Brown, K.; Frye, G. C.; Brinker, C. J. *J. Am. Chem. Soc.* **1989**, *111*, 7640–7649. (c) Bein, T. *Chem. Mater.* **1996**, *8*, 1636–1653, and references therein.
- (10) (a) Reis, K. P.; Joshi, V. K.; Thompson, M. E. *J. Catal.* **1996**, *161*, 62–67. (b) Newman, S. P.; Jones, W. *New J. Chem.* **1998**, *22*, 105–115.
- (11) O'Hare, D. *New J. Chem.* **1994**, *18*, 989–998, and selected references therein.
- (12) Russell, V. A.; Ward, M. D. *Chem. Mater.* **1996**, *8*, 1654–1666.
- (13) An elegant example of the principle was recently provided by Russell and co-workers [(a) Russell, V. A.; Etter, M. C.; Ward, M. D. *J. Am. Chem. Soc.* **1994**, *116*, 1941–1952. (b) Russell, V. A.; Evans, C. A.; Li, W.; Ward, M. D. *Science* **1997**, *276*, 575–580.] (not an organic–inorganic hybrid) in the formation of pillared 2D hydrogen-bonded molecular sandwiches wherein the co-assembly of guanidinium cations (G) and alkane-substituted sulfonate anions (SR) led to the formation of 2D quasi-hexagonal GS networks via directional hydrogen bonding between (G) NH–O(S) with a concomitant formation of the organic assemblies of R substituents in mono- or bimolecular motif.
- (14) Dance, I. G.; Fisher, K. J.; Banda, R. M. H.; Scudder, M. L. *Inorg. Chem.* **1991**, *30*, 183.
- (15) (a) Fijolek, H. G.; Grohal, J. R.; Sample, J. L.; Natan, M. J. *Inorg. Chem.* **1997**, *36*, 622–628. (b) Fijolek, H. G.; Pilar, G.-D.; Park, S. H.; Suib, S. L.; Natan, M. J. *Inorg. Chem.* **1997**, *36*, 5299–5305.
- (16) Baena, M. J.; Espinet, P.; Lequerica, M. C.; Levelut, A. M. *J. Am. Chem. Soc.* **1992**, *114*, 4182–4185.
- (17) A previous study (ref 15a) has suggested that the unstable trans (T) form of silver (butane) thiolates is white. The isomerization of the T form to the more stable gauche (G) form is accompanied by the color change from white to yellow. As will be later evident in this manuscript, we find no evidence of any significant population of the G form in colored crystallites of the longer-chain analogues examined here.
- (18) Snyder, R. G.; Schachtschneider, J. H. *Spectrochim. Acta* **1963**, *19*, 85–116.

- (19) Snyder, R. G.; Hsu, S. L.; Krimm, S. *Spectrochim. Acta, Part A* **1978**, *34*, 395–406.
- (20) MacPhail, R. A.; Snyder, R. G.; Strauss, H. L. *J. Chem. Phys.* **1982**, *77*, 1118–1130.
- (21) Hill, I. R.; Lewin, I. W. *J. Chem. Phys.* **1979**, *70*, 842–851.
- (22) MacPhail, R. A.; Strauss, H. L.; Snyder, R. G.; Elliger, C. A. *J. Phys. Chem.* **1982**, *88*, 334–341.
- (23) Snyder, R. G.; Strauss, H. L.; Elliger, C. A. *J. Phys. Chem.* **1982**, *86*, 5145–5150.
- (24) MacPhail, R. A.; Snyder, R. G.; Strauss, H. L. *J. Chem. Phys.* **1982**, *77*, 1118–1137.
- (25) Zerbi, G.; Roncoe, R.; Longhi, R.; Wunder, S. L. *J. Chem. Phys.* **1988**, *89*, 166.
- (26) Zerbi, G.; Abbate, S.; Gussoni, M. *J. Chem. Phys.* **1979**, *70*, 3577.
- (27) (a) Snyder, R. G. *J. Mol. Spectrosc.* **1961**, *7*, 116–173. (b) Casal, H. L.; Mantsch, H. H.; Cameron, D. G. *J. Chem. Phys.* **1982**, *77*, 2825–2830.
- (28) Nielsen, J. R.; Hathaway, C. E. *J. Mol. Spectrosc.* **1963**, *10*, 366.
- (29) Zerbi, G.; Magni, M.; Gussoni, M.; Moritz, K. H.; Bigotto, A.; Dirlikov, S. *J. Chem. Phys.* **1981**, *75*, 3175.
- (30) (a) Jones, R. N.; McKay, A. F.; Sinclair, R. G. *Philos. Trans. R. Soc. Chem.* **1952**, *A74*, 2575–2578. (b) Brown, J. K.; Sheppard, N.; Simpson, D. M. *Philos. Trans. R. Soc. Chem.* **1957**, *A247*, 35. (c) Snyder, R. G. *J. Mol. Spectrosc.* **1960**, *4*, 411–434. (d) Snyder, R. G. *J. Chem. Phys.* **1967**, *47*, 1316–1358.
- (31) Snyder, R. G.; Schaachtschneider, J. H. *Spectrochim. Acta, Part A* **1963**, *19*, 117–168.
- (32) (a) Maroncelli, M.; Qi, S. P.; Strauss, H. L.; Snyder, R. G. *J. Am. Chem. Soc.* **1982**, *104*, 6237–6247. (b) Snyder, R. G.; Maroncelli, M.; Qi, S. P.; Strauss, H. L. *Science* **1981**, *214*, 188–190. (c) Zerbi, G. In *Advances in Infrared and Raman Spectroscopy*; Clark, R. J. H., Hester, R. E., Eds.; Heyden: London, 1984.
- (33) The presence of non-trans conformation of the methylene group near the S headgroup due to geometric restrictions is not precluded here.
- However, the lack of peaks due to end-gauche conformers, suggests that a gauche structure of these methylenes is not formed in noticeable concentration.
- (34) Klug, H. P.; Alexander, L. E. *X-ray Diffraction Procedures for Polycrystalline and Amorphous Materials*; Wiley: New York, 1970.
- (35) (a) Douglas, B. E.; McDaniel, D. H.; Alexander, J. J. *Concepts and Models of Inorganic Chemistry*, 3rd Ed.; John Wiley: New York, 1994; p 102. (b) Streitwieser, A.; Heathcock, C. H. *Introduction to Organic Chemistry*; Macmillan: New York, 1976; pp 96–97.
- (36) Note that using assumed Ag–S bond lengths and S–S separation predicts a thickness of ~ 0.9 Å for the Ag–S slab.
- (37) Cullity, B. D. *Elements of X-ray Diffraction*; Addison-Wesley: Reading, MA, 1978.
- (38) In their model of distorted Ag–S lattice for silver butanethiolates, Fijolek and co-workers (ref 15a) note that, the slab thickness increases only marginally to accommodate end-gauche conformers.
- (39) (a) Block, E.; Gernon, M.; Kang, H.; Ofori-Okai, G.; Zubieta, J. *Inorg. Chem.* **1989**, *28*, 1263–1271, and selected references therein. (b) Dance, I. G. *Inorg. Chem.* **1981**, *20*, 1487–1492.
- (40) (a) Smith, A. E. *J. Chem. Phys.* **1953**, *21*, 2229–2229. (b) Broadhurst, M. G. *J. Res. Natl. Bur. Stand. Sect. A* **1962**, *66*, 241.
- (41) Muller, A. *Proc. R. Soc. London, Ser. A* **1932**, *138*, 514.
- (42) (a) Doucet, J.; Denicolo, A.; Craievich, A.; Collet, A. *J. Chem. Phys.* **1981**, *75*, 5125–5127. (b) Doucet, J.; Denicolo, A.; Craievich, A. *J. Chem. Phys.* **1981**, *75*, 1523–1529.
- (43) Our recent measurements of low-temperature IR spectra of silver thiolates further confirm that even at very low temperatures, splitting of the rocking and bending modes does not occur.
- (44) See, for example: *Micelles, Membranes, Microemulsions, and Monolayers*; Gelbert, W. M., Ben-Shaul, A., Rouz, D., Eds.; Springer: Berlin, 1994.